Article

FTIR Analysis of Changes in Chipboard Properties after Pretreatment with *Pleurotus ostreatus* (Jacq.) P. Kumm

Paweł Tryjarski [1], Jakub Gawron [2], Bogusław Andres [3], Agnieszka Obiedzińska [4]
and Aleksander Lisowski [1,*]

1   Department of Biosystems Engineering, Institute of Mechanical Engineering,
     Warsaw University of Life Sciences, Nowoursynowska 166, 02-787 Warsaw, Poland
2   Department of Production Engineering, Institute of Mechanical Engineering,
     Warsaw University of Life Sciences, Nowoursynowska 166, 02-787 Warsaw, Poland
3   Department of Wood Science and Wood Preservation, Institute of Wood Sciences and Furniture,
     Warsaw University of Life Sciences, Nowoursynowska 166, 02-787 Warsaw, Poland
4   Faculty of Computer Science and Food Science, Lomza State University of Applied Sciences, Lomza,
     Akademicka 14, 18-400 Łomża, Poland
*   Correspondence: aleksander_lisowski@sggw.pl

Abstract: A commercial three-layer particleboard served as model furniture for testing pretreatment with the oyster mushroom (*Pleurotus ostreatus* (Jacq.) P. Kumm.) over 9-, 12-, 16-, and 20-week periods based on the effects of reducing the enzymatic resistance of component cellulose. The effects of pretreatment were assessed based on Fourier-transform infrared spectroscopy (FTIR) of the treated particleboards, wherein indexes (peaks and peak ratios) connected with parameters influencing enzymatic cellulose hydrolysis were analysed. The data were analysed in two ways: the measurement of peak heights in both primary spectra and deconvoluted spectra. The peak heights for the determination of the total crystallinity index (*TCI*) were measured according to narrow and broad baselines. Time and how indexes are calculated were found to be the main factors significantly influencing the values of indexes of pretreatment in most cases. Until week 9, *P. ostreatus* pretreatment seems to be advantageous for biofuel production, which was illustrated by decreases in the intensity of the 1735 and 1505 cm^{-1} peaks and A_{1505}/A_{1735}, A_{1505}/A_{1375}, A_{1505}/A_{1158}, and A_{1505}/A_{896} ratios in addition to a reduction in crystallinity.

Keywords: wood waste; delignification; deconvolution; crystallinity changes; feature correlation method

1. Introduction

The issue of waste-particleboard valorisation originates from substantial development of the furniture industry in Poland. The demand for construction and furniture materials thus determines particleboard production, which reached 4.9 mln m^3 in 2018. For other similar boards from wood and wood-related materials, total production of the same year was nearly 5.9 mln m^3. Taking import into account, the amount of utilised materials of this group was close to 7 mln m^3, and production has since been increasing year by year [1].

Products of the furniture industry, including chipboard, have a limited lifespan, and after a certain period, some of them can be utilised in valorisation. Since particleboards are made from a lignocellulosic material—namely wood chips, which are glued with resin, usually urea–formaldehyde [2]—they can be utilised by conversion to biofuels [3].

Lignocellulosic materials offer the prospect of use as a second generation feedstock for commercial bioethanol production [4]. However, the production of bioethanol from lignocellulosic materials is hampered by enzyme resistance of this feedstock. It is thus advantageous to pretreat such materials prior to their conversion to bioethanol. Pretreatment of lignocellulosic material is an important step in the biological processing of cellulose. It

aims to prepare the raw material for enzymatic decomposition. This is achieved by separating lignin and hemicelluloses from cellulose, as well as increasing the raw material porosity and decreasing the cellulose crystallinity [4]. The removal of lignin from loblolly pine wood (*Pinus taeda*) by enzymatic hydrolysis results in the physicochemical modification of the cell-wall structure, which in turn facilitates enzymatic access to cellulose [5]. In contrast, the crystallinity of cellulose has a negative effect on its enzymatic hydrolysis dynamics, and the latter are linearly related to the amount of cellulose.

Based on the results from the enzymatic hydrolysis of *Miscanthus sinensis*, it was found that reducing the crystallinity of the material also increased the hydrolysis efficiency during the initial stage. The initial hydrolysis efficiency is related to the access of cellulose hydrolysing enzymes to the substrate, and this in turn depends on the particle size of the biomass [6]. Substrate delignification and xylanase supplementation allow complete hydrolysis of hemicelluloses to monosaccharides in the <150 µm fraction of *Miscanthus sinensis*, and glucan to glucose conversion can reach 91%. However, cellulase activity can still be suppressed by residual lignin in the material following delignification [6].

After a 15-day biological treatment of rapeseed straw with *Phanerochaete chrysosporium*, the hydrolysis ratio increased from 2.2% to 6.6% despite an increase in crystallinity from 33.17% to 39.47%. This increase in crystallinity was associated with the removal of lignin and hemicelluloses. Biological pretreatment reduced the enzymatic hydrolysis rate. A linear relationship was found between the hydrolysis ratio and lignin distribution. However, both lignin loss (6.18%) and the hydrolysis ratio were low [7].

In the catalytic hydrogenolysis of biomass, delignification level and glucose yield are shown to be correlated. Lignin removal during hydrogenolysis is correlated with glucose yield, and the inclusion of lignin depolymerisation catalysts significantly improves lignin removal and enzymatic hydrolysis efficiency [8].

In another experiment, no selective loss of lignin was observed, yet the degree of glucan–glucose conversion increased. This was for conversion of the glucose content of the hydrolysate and the anhydroglucose content of the biomass. Pretreatment of pine wood with ionic liquids did not change the lignin content, and the degree of glucan conversion to glucose increased from 5% to as much as 84%. It is presumed that the increased conversion may be due to changes in the spatial distribution of lignin. The increase in glucan conversion efficiency has also been linked to an increase in the porosity of the test material (pores with diameters of 5−202 nm) and an increase in the accessible surface area of the material due to the ionic liquid treatment [9].

The yield of glucose extraction during enzymatic hydrolysis is influenced not only by the lignin itself but also by the proportions of different lignin-building monomers, i.e., syringyl, *S*, and guaiacyl, *G*. In poplar *Populus trichocarpa* wood, both native and hot-water pretreated, a higher S/G ratio value was found to be associated with a higher glucose yield from the raw material [10]. Similarly, a higher sugar yield was found to be positively correlated with the S/G ratio in different variants of willow *Salix viminalis* L. after their high-throughput pretreatments [11]. In the analysis of different eucalyptus samples, no statistically significant correlation was found between glucose and xylose yield and S/G ratio, regardless of whether pretreatment had taken place [12]. *G* is shown to have a greater capacity for enzyme adsorption than *S* [13], and the amount of *S* alone does not appear to positively influence the conversion rate of cellulose to glucose [14].

Lignin monomers *S* and *G* have different susceptibility for pretreatment methods. The higher lignin content caused by hemicellulose removal during pretreatment seems to be more important than lignin removal during the creation of pores allowing access of cellulases [15]. In poplar and eucalyptus wood, increases in S/G ratios are associated with a considerable reduction in lignin content [16]. Substrates richer in lignin usually have a higher S/G ratio and are more vulnerable for delignification, because *S* forms less stable bonds than *G* [17]. However, the relationship between the S/G value and the release of sugars has not been clearly explained.

The removal of hemicelluloses also increases the enzymatic decomposition of cellulose. It was observed that, after carrying out the delignification of poplar with $NaClO_2$ at an elevated temperature, the cellulose conversion rate was 68.2% after 34 h of enzymatic hydrolysis. After delignification, the removal of hemicellulose with diluted NaOH allowed for the enzymatic degradation of 75.2% its constituent cellulose [18].

Factors influencing enzymatic hydrolysis have been analysed using various techniques and technologies. One of the cheapest and most environmentally friendly pretreatment technologies involves the utilisation of white rot fungi. As an example, corn straw was pretreated with six white rot species, and higher lignin removal (38.3%) was achieved after a 25-day pretreatment with *Pleurotus sajor-caju*. The hydrolysis yield reached 71.2% in 60 h. The ethanol yield from cellulose with *Candida utilis* yeast fermentation was 42.1% of the theoretical limit. The ethanol yield was lower than with *Saccharomyces cerevisiae*, which is usually around 50% of the theoretical value; however, after ethanol distillation, a byproduct with a higher protein content was obtained [19]. Compared with physicochemical methods, biological pretreatment with white rot fungi is a long and less efficient process. For example, 20 min $FeCl_3$ pretreatment allowed a 98% hydrolysis yield. Physicochemical methods are, however, expensive and put a burden on the environment [19] as well, in addition to causing the formation of larger amounts of byproducts that inhibit yeast growth, such as furfural, 5-hydroxymetylofurfural, and phenol [20].

Some researchers have suggested combining biological and physicochemical pretreatment [19]. Two stage pretreatment of Chinese white poplar *Populus tomentosa* with fungus *Lenzites betulina* (L.) Fr. and hot water increased the glucose yield by 2.25 compared with sole biological pretreatment [19]. Pretreatment of California pine *Pinus radiata* with steam explosion pretreatment, followed by 12 weeks with *Trametes versicolor* (L.) Lloyd, removed 13% of lignin and increased the glucose yield 6-fold [21].

Gravimetric analysis, Fourier-transform infrared spectroscopy (FTIR), and nuclear magnetic resonance spectroscopy were used in one study for compound identification and to observe intramolecular changes and changes in the chemical composition of wood during fungal pretreatment [22]. FTIR is a useful technique because it allows the analysis of small amounts of wood samples. Most published articles describe qualitive changes in FTIR spectra during long time periods. Information about changes in spectra during a shorter fungal decay of particleboard are scant.

In the available literature, data about the biological pretreatment of particleboard waste for ethanol production are lacking.

The aim of our study was to assess the utilisation of the oyster mushroom, *Pleurotus ostreatus* (Jacq.) P. Kumm., a white rot fungus, in the pretreatment of commercial particleboards. Pretreated material was analysed by FTIR to assess changes in parameters connected with the ethanol yields of lignocellulosic materials.

The choice of *P. ostreatus* for waste particleboard pretreatment was inspired by the results of switchgrass (*Panicum virgatum* var. Kanlow) pretreatment with this mushroom [23]. Moreover, *P. ostreatus* is an easily accessible and versatile mushroom as it grows on all continents except Antarctica and is the second most cultivated edible mushroom after *Agaricus bisporus* [24]. *P. ostreatus* has the potential to be utilised in many ways, such as the mycoremediation of landfill leachate [25] and soil [26], the decomposition of textile dying effluents [27], enzymes production [28] and forage valorisation [29].

The results of particleboard pretreatment with *P. ostreatus* were estimated based on the total crystallinity index, TCI; lateral order index, LOI; relative lignin content, LC; delignification against polysaccharides; and changes in absorbance for characteristic peaks of lignin/carbohydrates.

The relative intensities of peaks characteristic for lignin/carbohydrates were interpreted based on information from the literature. The absorbance values of wavenumbers characteristic for chemical compounds are shown in Table 1.

Table 1. Wavenumbers and their assignments.

Wavenumber cm^{-1}	Assignment	Reference
2900	C–H and CH$_2$ stretching	[30]
1735	unconjugated C=O in xylans (hemicellulose) [22]; unconjugated C–O in acetyl group (xylan in hardwoods, glucomannan in softwoods) [31]	[22,31]
1505	aromatic skeletal in lignin [22]; aromatic skeletal vibration C=C [31]; stretching modes of benzene ring in lignin [32]	[22,31,32]
1420	CH$_2$ scissoring motion [30]; CH$_2$ scissor vibration in cellulose and CH bonds in methoxyl groups in lignin [32]; C–H deformation in lignin and carbohydrates [22]; C–H in plane deformation with aromatic ring stretching, in lignin [31]	[22,31,32]
1375	CH bending modes in cellulose and hemicellulose [32]; C–H bending mode [30]; C–H deformation in cellulose and hemicellulose [31]; CH stretching in CH$_2$ in urea–formaldehyde resin [33]	[30–33]
1158	C–O–C vibration in cellulose and hemicellulose	[31]
1120	aromatic skeletal and C–O stretching	[34]
1078	C–O stretch in cellulose and hemicellulose	[34]
896	C–H deformation in cellulose [22]; vibrational mode involving C1 and the four atoms attached to it [32]	[22,32]

2. Materials and Methods

2.1. Sample Preparation and Pretreatment

The three-layer particleboard produced by Swiss Krono (Żary, Poland) was made of wood shavings blending mainly from tree species: *Pinus* (78%), *Picea* (11%), *Betula* (4.5%), *Populus* (2%), *Alnus* (1.5%) and *Larix* (1%). The remaining species, *Tilia*, *Acer* and *Pseudotsuga*, constituted a total of 2%. The particleboard was cut perpendicular to the surface in 50 mm × 16 mm × 16 mm samples. Next, samples were sterilised in a polypropylene bag for 30 min at 121 °C and under 1 bar of pressure.

Malt extract agar medium was poured into 0.5 L glass containers with lids and a cotton gauze/cellulose wool seal to enable air diffusion. Containers were sterilised in the abovementioned conditions.

P. ostreatus inoculum, not older than 2 weeks and in the active growth phrase, was transferred from slants into containers. The containers were placed in a bacteriological incubator (Incudigit 80, JP Selecta, Barcelona, Spain) at 24 °C until mycelium covered the surface of the agar medium. An additional dish with water was placed into the incubator to maintain air humidity at 80–90% RH for fungal growth.

In each container, four sterile particleboard samples were put onto the mycelium surface according to the cut plane. This sample orientation was chosen to more readily facilitate fungal growth. Samples in closed, gauze/wool sealed containers were incubated in an incubator at 24 ± 1 °C. Air humidity was maintained using a dish with water, as mentioned above. Samples were taken after 9, 12, 16, and 20 weeks; oven dried at 105 °C; and left in zipped bags for further analysis.

2.2. Research Procedure

Half of the samples from each time interval were milled in a laboratory knife mill (LNM100, Testchem Ltd., Warsaw, Poland) operated at a 2870 rpm rotational speed, equipped with 3 high speed steel knives and a 0.425 mm sieve. Milled samples were put back into bags with unmilled material.

Milled samples were analysed with an IR spectrophotometer (IRAffinity1S, Kyoto, Japan) using an ATR accessory. Each sample was scanned in 3 spots. Each spot was scanned 32 times with 4 cm^{-1} spectral resolution in the 4000−400 cm^{-1} range. Spectra

were processed with OMNIC^{TM} 8 software (Thermo Fisher Scientific, Waltham, MA, USA). Before further analysis, spectra were smoothed with the 9-point Savitzky–Golay algorithm.

Before deconvolution, each spectrum was divided in 3 ranges. Range I—around the peak characteristic for CH vibrations, about 2900 cm^{-1}; range II—the whole region between 1750 and 1200 cm^{-1}; and range III—a region between 1200 and 840 cm^{-1} (Figure 1). Spectra were divided because it was impossible to deconvolute them as a whole while also maintaining the appropriate algorithmic sensitivity. Ranges were chosen to avoid the influence of the division of peaks after deconvolution.
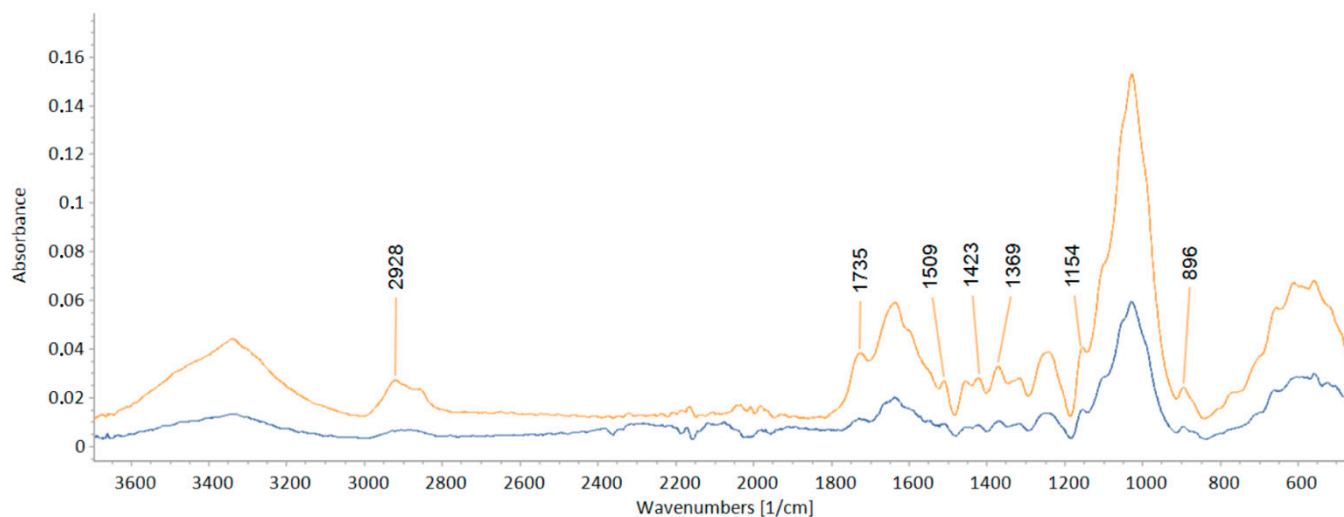

Figure 1. An example of FTIR spectra of particleboard before (blue line) and after (brown line) 20 weeks of deconvolution with *P. ostreatus*; I–III—separated ranges of spectra; the selected wavenumbers are described in Table 1.

Spectra were deconvoluted using the Fletcher–Powell–McCormick algorithm with high sensitivity. Peaks of Gaussian shape and full width at half maximum of 5 cm^{-1} were assumed. The threshold for noise was individually determined for each part of the spectra.

Analysed indexes were calculated based on absorbance peak heights in deconvoluted spectra, where individual peaks were chosen based on the authors' experience as the nearest to those representing the actual chemical bonds of interest in the literature.

2.3. Indexes for Evaluation of Pretreatment

Particleboard pretreatment was evaluated according to the following indexes:

(1) Changes in lignin content—evaluated by changes in absorbance for aromatic rings in lignin (A_{1505}).

(2) Delignification selectivity—calculated as a change in the absorbance of wavenumber characteristic for lignin against the absorbance of wavenumbers characteristic for polysaccharides: hemicelluloses, holocellulose, and cellulose. Relative lignin content is shown by Equation (1), which is a modified version of an equation from another study [31].

$$LC_r = \frac{A_{1505}}{A_{CH}} \tag{1}$$

where LC_r is the relative lignin content; A_{1505} is the absorbance of wavenumber characteristic for lignin 1505 cm^{-1}; A_{CH} is the absorbance of wavenumbers characteristic for cellulose at 896 cm^{-1}, holocellulose at 1158 and 1375 cm^{-1}, and acetyl groups in hemicelluloses at 1734 cm^{-1}.

The peak positions were chosen as for hardwoods in [22], because this article describes the decay of sole wood, not wood-high density polyethylene composition, as in [31].

(3.1) Lateral order index, *LOI*, introduced by O'Connor [35], calculated as a A_{1420} to A_{896} ratio.

$$LOI = \frac{A_{1420}}{A_{896}} \tag{2}$$

where *LOI* is the lateral order index; A_{1420} is the absorbance of the peak for wavenumber 1420 cm^{-1}, characteristic for CH$_2$ scissoring vibration assigned to crystalline fraction (amount of crystalline cellulose is connected with "crystallinity peak", around 1420–1430 cm^{-1}); A_{896} is the absorbance of the peak at wavenumber 896 cm^{-1}, which is characteristic for C–O–C β-(1,4)-glycosidic stretching vibrations assigned to the amorphous fraction (peak around 893–898 cm^{-1} is referred to as the amorphous peak) [36].

(3.2) Total crystallinity index, *TCI*, defined by Nelson and O'Connor [30] based on the ratio of absorbances of peaks at 1372 and 2900 cm^{-1}.

$$TCI = \frac{A_{1375}}{A_{2900}} \tag{3}$$

where TCI is the total crystallinity index, A_{2900} is the absorbance of the peak at wavenumber 2900 cm^{-1}, characteristic for CH$_2$ stretching vibrations, assigned to the amorphous fraction; A_{1375} is the absorbance of the peak at wavenumber 1375 cm^{-1}, characteristic for CH bending vibrations.

Differently than other indexes, *TCI* was computed from the heights of respective peaks with individually chosen baselines (named narrow baselines) and heights of respective peaks obtained from spectra deconvolution, and an additional ratio was computed on the basis of the height of the 1375 cm^{-1} peak with a baseline common for a group of peaks, similarly to some research for pure cellulose [30], e.g., between 1400 and 1290 cm^{-1} (named broad baseline). A_{2900}, a denominator in TCI, was the same for A_{1375} with narrow and broad baselines.

(3.3) Crystallinity R—calculated as a ratio of absorbances of peaks 1120–1078 cm^{-1}; when the ratio R increases, crystallinity decreases [37].

$$R = \frac{A_{1120}}{A_{1078}} \tag{4}$$

where *R* is the crystallinity, A_{1120} is the absorbance of the peak for wavenumber 1120 cm^{-1} characteristic for CH bending, and A_{1078} is the absorbance of the peak for wavenumber 1078 cm^{-1} characteristic for C–O–C stretching in a pyranose ring.

Each of the indexes was calculated based on the height of absorbance peaks and on spectral deconvolution. No A_{1327} and A_{1272} peaks were observed, so the *S/G* ratio was not calculated.

2.4. Selection of Indexes

Indexes measured during the pretreatment of particleboard with *P. ostreatus* were selected by a feature correlation method, and strong correlated indexes were eliminated. The aim of this was to reduce the number of indexes to the suggested 7 ± 2 [38] and thus reduce the amount of laborious manual information processing required.

The selection of indexes was initiated by first preparing a correlation coefficient matrix **R** for these indexes and later converting this to an inverted matrix $\mathbf{R}^{-1}$, $\mathbf{R}^{-1} = \mathbf{R}^{T}/\det(\mathbf{R})$, where $\mathbf{R}^{T}$ is a transpose of matrix **R**, and det(**R**) is a determinant of matrix **R** (det(**R**) $\neq 0$ is required). When an index was strongly correlated with others, elements of $\mathbf{R}^{-1}$ exceeded 10, and numerical determination of the matrix was wrong. An index was removed from the primary set of indexes if the diagonal value was ≥10. After the removal of one index, the procedure was repeated again and again until the diagonal value was <10. Results were

checked by calculating identity matrix $\mathbf{I}$; $\mathbf{I} = \mathbf{R} \cdot \mathbf{R}^{-1}$. Correlation coefficient matrix $\mathbf{R}$ was calculated in Statistica v.13.3 (StatSoft Ltd., Cracow, Poland) and det($\mathbf{R}$) and $\mathbf{I}$ in Excel.

2.5. Statistical Analysis

For each of the indexes of pretreatment, the normality of distribution was checked with the following tests: Kolmogorov–Smirnov (K–S) with Lilliefors correction (K–S–L) and Shapiro–Wilk (S–W). The homogeneity of variance for the values of pretreatment indexes measured with peak height and deconvolution methods was checked with Levene and Brown–Forsythe tests. Less favourable results were obtained for K–S–L and S–W tests, although only in 8 of 145 cases. K–S test results did not allow rejection of the H_0 hypothesis that pretreatment index values were normally distributed. For most of the indexes, the H_0 hypothesis, namely homogeneity of variance, could not be rejected on the basis of the Levene and Brown–Forsyth tests. Absorbances for wavenumber 1158 cm^{-1} and TCI p-values indicated that the results were not significant at the level of 0.05 (0.007 and 0.003, respectively)—any conclusion based on ANOVA results should thus be taken with caution.

The influences of pretreatment time and methods for calculating indexes (height and deconvolution), along with differentiation of indexes, for particleboard pretreatment with *P. ostreatus* were analysed using ANOVA and F (Fisher–Snedecor) tests. Detailed analyses of average indexes were tested conducted using the Turkey test. Correlation coefficients were also subjected to analysis based on a Pearson matrix. For correlation coefficient values, descriptor synonyms were used [39]. The significance of both coefficients' influences on indexes and the differences between average indexes were analysed for critical value $p = 0.05$. The statistical analysis of the results of the research was conducted with the Statistica v.13.3 software (StatSoft Poland Ltd., Cracow, Poland).

3. Results and Discussion

The results of the analysis of variance and the mean values and standard deviations of the analysed indexes are shown in Table 2; the corresponding matrix of correlation coefficients is in Table 3.

The results of the analysis of variance and the mean values and standard deviations of analysed indexes are shown in Table 2; the corresponding matrix of correlation coefficients is in Table 3.

The main factors, e.g., time and methods for the calculation of indexes, were, in most cases, statistically significant variables describing the variability of indexes during particleboard pretreatment with *P. ostreatus*. Statistically insignificant against the time of pretreatment were variability in absorbance at wavenumbers 1375 cm^{-1} ($p = 0.083$) and 1420 cm^{-1} ($p = 0.118$) and *TCI* value ($p = 0.305$), and against method of calculation were the variability of A_{1505}/A_{1735}, A_{1505}/A_{896} ratios and absorbance for wavenumber 1375 cm^{-1} (for *board base*), with p-values of 0.738, 0.468 and 0.425, respectively. The interaction of the main factors significantly influenced the variability in absorbances for wavenumbers 505, 1735 and 1375 cm^{-1} (for *broad base*) and A_{1505}/A_{1375} and A_{1505}/A_{1158} ratios and the *TCIb* (for *broad base*) ratio.

Changes in the described indexes of particleboard pretreatment with *P. ostreatus* are presented in the following subsections.

3.1. Delignification

In week 9, the value of A_{1505} (Figure 2), caused by vibrations in aromatic rings in lignin and vibrations in formaldehyde, decreased (on average from 0.016 to 0.010), which indicates lignin degradation by *P. ostreatus* (Figure 3). In week 12, A_{1505} increased, perhaps as a result of formaldehyde production during the degradation of methoxyl groups in lignin by the fungus [40], and this assumption is supported by an increase in A_{1735} (Figure 3), because peak 1735 cm^{-1} is present in the formaldehyde spectrum [41]. Formaldehyde production may compensate for a decrease in A_{1505} caused by lignin degradation.

Table 2. Results of the analysis of variance and the mean values and standard deviations (SDs) of indexes of particleboard pretreatment with *P. ostreatus*.

F **	A_{1505}	A_{1735}	A_{1505}/A_{1735}	A_{1505}/A_{1375}	A_{1505}/A_{1158}	A_{1505}/A_{896}	$A_{1375}b$	$A_{1375}n$	A_{1158}	A_{896}	LOI	A_{1420}	A_{2900}	TCIb	TCIn	A_{1120}/A_{1078}
p																
t	<0.001	<0.001	<0.001	<0.001	<0.001	<0.001	<0.001	0.083	0.028	0.015	0.021	0.118	0.006	0.003	0.307	0.005
M	<0.001	<0.001	0.738	<0.001	<0.001	0.468	0.425	ND	<0.001	<0.001	0.003	0.003	0.004	<0.001	ND	ND
t × M	<0.001	<0.001	0.774	0.032	0.015	0.115	<0.001	ND	0.792	0.714	0.094	0.183	0.594	0.013	ND	ND
	$A \pm SD$	$A \pm SD$	$A \pm SD$	$A \pm SD$	$A \pm SD$	$A \pm SD$	$A \pm SD$	$A \pm SD$	$A \pm SD$	$A \pm SD$	$A \pm SD$	$A \pm SD$	$A \pm SD$	$A \pm SD$	$A \pm SD$	$A \pm SD$
t, w																
0	0.016 [c,*] ± 0.002	0.006 [b] ± 0.001	2.54 [b] ± 0.3	2.41 [c] ± 0.4	1.49 [c,d] ± 0.6	2.37 [c] ± 0.56	0.007 [a,b] ± 0.001	0.006 [a] ± 0.001	0.012 [a,b] ± 0.005	0.007 [a,b] ± 0.001	1.22 [a,b] ± 0.34	0.008 [a] ± 0.001	0.005 [a] ± 0.001	1.45 [a,b] ± 0.3	0.99 [a] ± 0.05	0.75 [b] ± 0.01
9	0.010 [c] ± 0.002	0.006 [b] ± 0.002	1.75 [a] ± 0.12	1.42 [a,b] ± 0.24	1.14 [b,c] ± 0.3	1.65 [b] ± 0.16	0.007 [a,b] ± 0.001	0.005 [a] ± 0.001	0.009 [a] ± 0.004	0.006 [a] ± 0.002	1.07 [a,b] ± 0.1	0.006 [a] ± 0.001	0.005 [a] ± 0.001	1.49 [a,b] ± 0.29	1.05 [a] ± 0.08	0.61 [a,b] ± 0.14
12	0.016 [b] ± 0.004	0.009 [c] ± 0.002	1.73 [a] ± 0.1	1.73 [b] ± 0.09	1.65 [d] ± 0.31	2.62 [c] ± 0.31	0.009 [c] ± 0.002	0.006 [a] ± 0.001	0.010 [a,b] ± 0.004	0.006 [a] ± 0.002	1.31 [b] ± 0.12	0.008 [a] ± 0.001	0.006 [a,b] ± 0.001	1.65 [b] ± 0.54	1.00 [a] ± 0.08	0.51 [a] ± 0.03
16	0.011 [b] ± 0.004	0.006 [b] ± 0.002	1.96 [a] ± 0.49	1.43 [a,b] ± 0.69	0.79 [a,b] ± 0.13	1.36 [a,b] ± 0.35	0.008 [b,c] ± 0.002	0.007 [a] ± 0.001	0.014 [b] ± 0.005	0.008 [b] ± 0.002	1.01 [a] ± 0.22	0.008 [a] ± 0.002	0.007 [b] ± 0.001	1.21 [a] ± 0.2	0.94 [a] ± 0.19	0.50 [a] ± 0.04
20	0.006 [a] ± 0.002	0.004 [a] ± 0.001	1.46 [a] ± 0.32	1.13 [a] ± 0.59	0.55 [a] ± 0.15	0.84 [a] ± 0.19	0.005 [a] ± 0.001	0.005 [a] ± 0.001	0.011 [a,b] ± 0.005	0.007 [a,b] ± 0.003	1.03 [a,b] ± 0.13	0.007 [a] ± 0.002	0.005 [a] ± 0.002	1.23 [a] ± 0.17	0.85 [a] ± 0.13	0.53 [a] ± 0.11
M																
h	0.010 [a] ± 0.004	0.005 [a] ± 0.002	1.91 [a] ± 0.45	1.44 [a] ± 0.65	1.35 [b] ± 0.62	1.87 [a] ± 0.82	0.007 [a] ± 0.002	0.006 ± 0.001	0.008 [a] ± 0.002	0.005 [a] ± 0.001	1.24 [b] ± 0.2	0.007 [a] ± 0.001	0.006 [b] ± 0.001	1.20 [a] ± 0.12	0.97 ± 0.12	ND
d	0.014 [b] ± 0.005	0.007 [b] ± 0.002	1.95 [a] ± 0.53	1.91 [b] ± 0.53	0.95 [a] ± 0.37	1.74 [a] ± 0.67	0.007 [a] ± 0.002	ND	0.015 [b] ± 0.004	0.008 [b] ± 0.001	1.02 [a] ± 0.22	0.008 [b] ± 0.002	0.005 [a] ± 0.001	1.61 [b] ± 0.37	ND	0.59 ± 0.12

* Means with the different letters in the same column are significantly different ($p \leq 0.05$) by Tukey's multiple range test. ND: not determined. ** F—factor; *p*—*p*-value; *t*—time; *M*—method; w—week; *A*—average value; *SD*—standard deviation; *h*—height; *d*—deconvolution; *b*—broad base; *n*—narrow base; A_{896}, A_{1158}, A_{1375}, A_{1420}, A_{1505}, A_{1735}, and A_{2900}—absorbance for wavenumbers characteristic for cellulose 896 cm^{-1}, holocellulose 1158 cm^{-1} and 1375 cm^{-1}, crystalline fraction 1420 cm^{-1}, lignin 1505 cm^{-1}, hemicelluloses (acetyl groups) 1735 cm^{-1}, and amorphous fraction 2900 cm^{-1}, respectively; A_{1505}/A_{896}, A_{1505}/A_{1158}, A_{1505}/A_{1375}, and A_{1505}/A_{1735}—relative lignin content against cellulose A_{896}, holocellulose A_{1158} and A_{1375}, and hemicelluloses A_{1735}, respectively; *LOI*—lateral order index; *TCI*—total crystallinity index.

Table 3. Pearson matrix of correlation coefficients for indexes of particleboard pretreatment with *P. ostreatus*.

Parameter	A_{1505}	A_{1735}	A_{1505}/A_{1735}	A_{1505}/A_{1375}	$A_{1375}b$	A_{1505}/A_{1158}	A_{1158}	A_{1505}/A_{896}	A_{896}	LOI	A_{1420}	TCIb	A_{2900}
A_{1505}	1.000												
A_{1735}	0.803[a]	1.000											
A_{1505}/A_{1735}	0.615[a]	0.042	1.000										
A_{1505}/A_{1375}	0.755[a]	0.356[a]	0.825[a]	1.000									
$A_{1375}b$	0.473[a]	0.664[a]	−0.085	−0.188	1.000								
A_{1505}/A_{1158}	0.502[a]	0.365[a]	0.378[a]	0.390[a]	0.195	1.000							
A_{1158}	0.425[a]	0.373[a]	0.221	0.393[a]	0.132	−0.498[a]	1.000						
A_{1505}/A_{896}	0.769[a]	0.597[a]	0.506[a]	0.586[a]	0.326	0.912[a]	−0.190	1.000					
A_{896}	0.307	0.322	0.108	0.257	0.163	−0.528[a]	0.931[a]	−0.315	1.000				
LOI	0.288	0.186	0.227	0.148	0.206	0.772[a]	−0.524[a]	0.699[a]	−0.579[a]	1.000			
A_{1420}	0.618[a]	0.537[a]	0.330	0.403[a]	0.425[a]	0.011	0.624[a]	0.217	0.641[a]	0.225	1.000		
TCIb	0.522[a]	0.584[a]	0.116	0.303	0.377[a]	0.103	0.288	0.342	0.193	0.033	0.333	1.000	
A_{2900}	−0.002	0.112	−0.169	−0.436[a]	0.618[a]	0.083	−0.120	0.010	−0.010	0.133	0.085	−0.476[a]	1.000

[a]—Statistically significant value of correlation coefficient for $p = 0.05$. A_{896}, A_{1158}, A_{1375}, A_{1420}, A_{1505}, A_{1735}, and A_{2900}—absorbance for wavenumbers characteristic for: cellulose 896 cm^{-1}, holocellulose 1158 cm^{-1} and 1375 cm^{-1}, crystalline fraction 1420 cm^{-1}, lignin 1505 cm^{-1}, hemicelluloses (acetyl group) 1735 cm^{-1}, and amorphous fraction 2900 cm^{-1}, respectively; A_{1505}/A_{1158}, A_{1505}/A_{1375}, and A_{1505}/A_{1735}—relative lignin content against cellulose A_{896}, holocellulose A_{1158} and A_{1375}, and hemicelluloses A_{1735}, respectively; *LOI*—lateral order index; *TCI*—total crystallinity index; *b*—broad base.
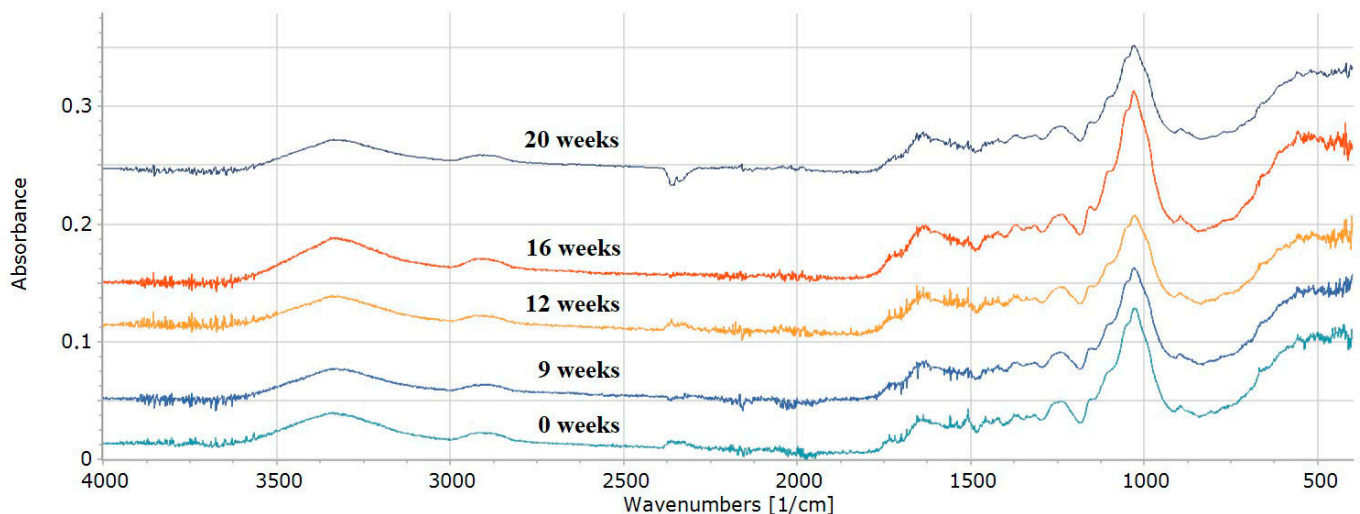
Figure 2. FTIR spectra for selected particleboard samples after 0, 9, 12, 16, and 20 weeks pretreatment with *P. ostreatus*.

In weeks 16 and 20, the expected successive decrease in A_{1505} resulting from lignin degradation appears (Figure 2); however, changes in A_{1735}, A_{1505}, and A_{896} during the whole experiment do not point to an exclusive role of formaldehyde, as changes in the absorbances of these peaks do not present the same trend. This is clearly visible from the lack of correlation between A_{1735} and A_{896} and between A_{1505} and A_{896}, whereas A_{1735} and A_{1505} are highly correlated (r = 0.803), Table 3. The sources of changes in values for these wavenumbers should be investigated in further research.

The change in the A_{1505} value resulting from deconvolution is in line with that of peak height but with a higher mean value, amounting to 0.014 and 0.010, respectively (Table 2). Deconvolution of spectra allowed for excluding changes in absorbance caused by changes in the heights of neighbour peaks.
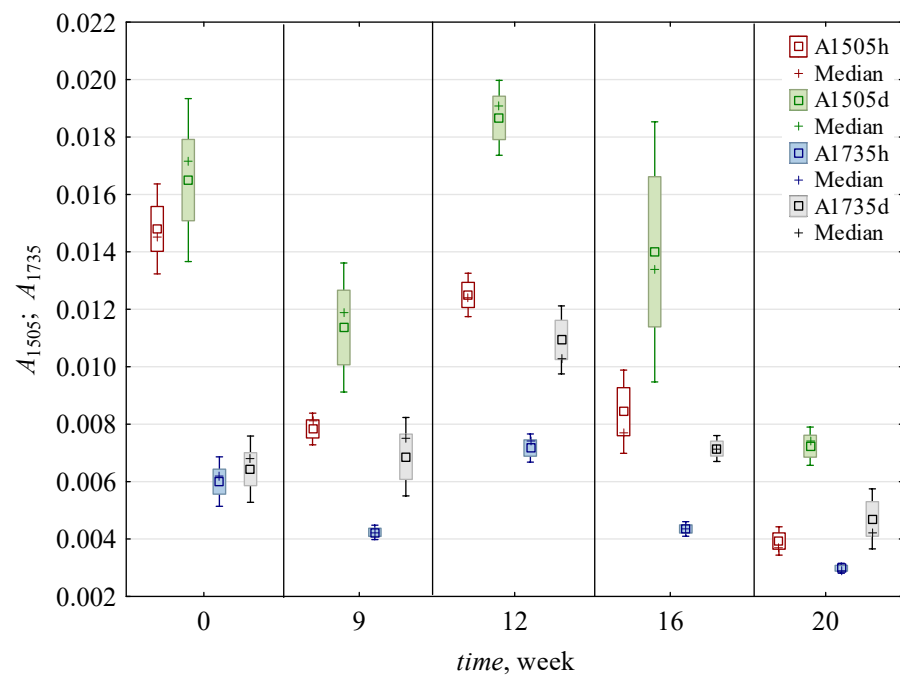
Figure 3. Value of absorbance A_{1505} for wavenumber characteristic for lignin and A_{1735} for hemicelluloses; h—peak height, d—peak deconvolution, □—mean, frame—standard error (*SE*), and whisker—standard deviation (*SD*).

3.2. Delignification Based on Comparison with Polysaccharides

In week 9, the A_{1505}/A_{1735}, A_{1505}/A_{1375}, A_{1505}/A_{1158}, and A_{1505}/A_{896} ratios decreased (Figures 3 and 4), which indicates selective degradation of lignin over hemicelluloses, holocellulose, and cellulose. From week 12, the tendency of changes in the A_{1505}/A_{1735} ratio differed from those of other ratios. The A_{1505}/A_{1375}, A_{1505}/A_{1158}, and A_{1505}/A_{896} ratios increased between weeks 9 and 12 and later decreased until week 20.
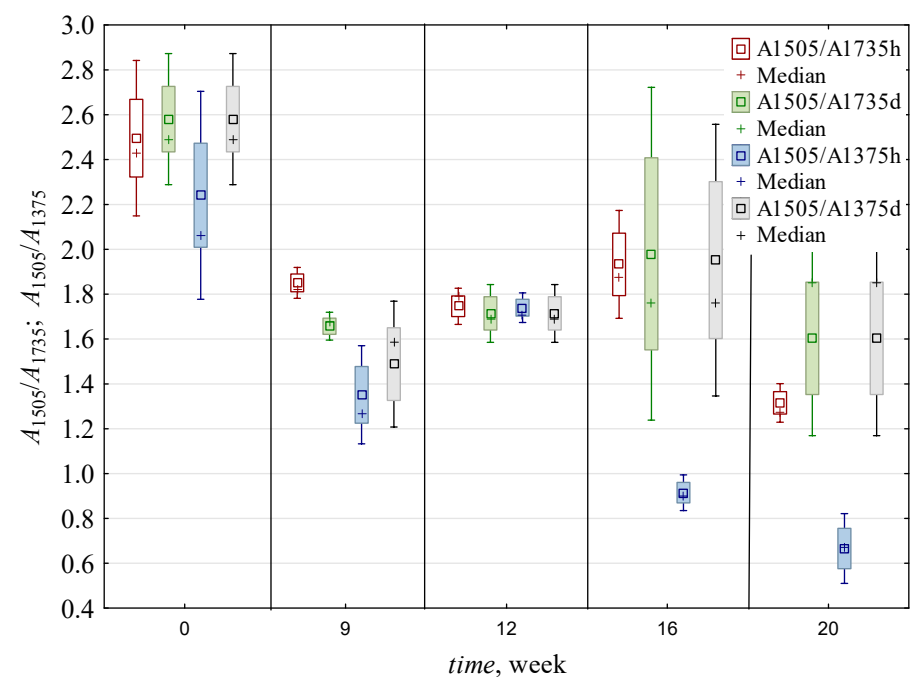

Figure 4. Values of ratios of absorbances for respective wavenumbers: A_{1505}/A_{1735} and A_{1505}/A_{1375}; h—peak height, d—peak deconvolution, □—mean, frame—*SE*, and whisker—*SD*.

3.2.1. Delignification Based on Comparison with Hemicelluloses

In week 9, A_{1505}/A_{1735} decreased and later plateaued (Figure 4). The initial decrease was caused mainly by a decrease in A_{1735}, which might be a result of hemicellulose degradation by *P. ostreatus*. The further plateau was a result of simultaneous changes in ratio A_{1505}/A_{1735}, and the absolute values are presented in Figure 3.

3.2.2. Delignification Based on Comparison with Holocellulose

The A_{1505}/A_{1375} ratio, related to the amount of lignin compared with hemicelluloses, decreased during the experiment, which may indicate selective delignification in preference to degradation of hemicelluloses (Figure 4).

The decrease in A_{1505}/A_{1375}, for both peak heights and deconvolution, was overestimated due to an increase in the value of A_{1375} in week 16 (Figure 5), and these changes could be caused by the appearance of metabolites and further removed in week 20. Peak A_{1375} (Figure 2) also originated from C–H w CH_2 vibrations in urea–formaldehyde resin [33], so resin degradation might cause an increase in the A_{1505}/A_{1375} ratio.
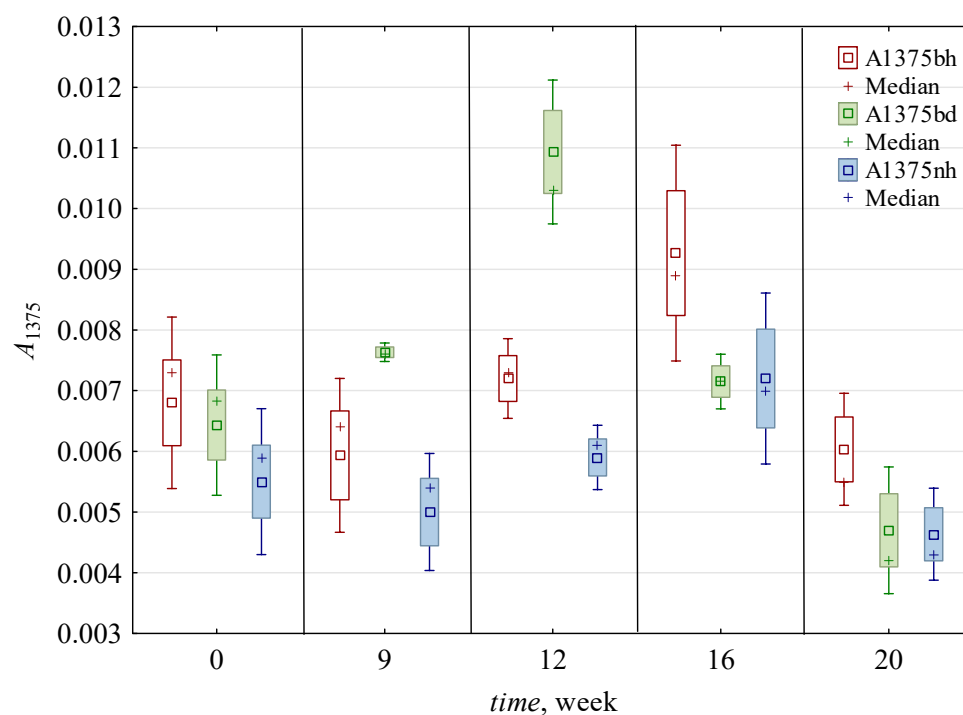

Figure 5. Value of absorbance A_{1375} for wavenumber characteristic for holocellulose; *b*—broad base, *n*—narrow base, *h*—peak height, *d*—peak deconvolution, □—mean, frame—*SE*, and whisker—*SD*.

The A_{1505}/A_{1158} ratio (Figure 6), similar to A_{1505}/A_{1375}, indicates the amount of lignin compared with holocellulose and presents the same tendency.

Absorbance for peak A_{1158} decreased in week 9 (on average from 0.012 to 0.009, Table 2), successively increased until week 16 (up to 0.014), and finally decreased (to 0.011, Figure 7) in week 20. During the experiments, values from deconvolution had similar oscillations as heights, although absolute values were almost twice those of 0.015 and 0.008, respectively (Table 2).
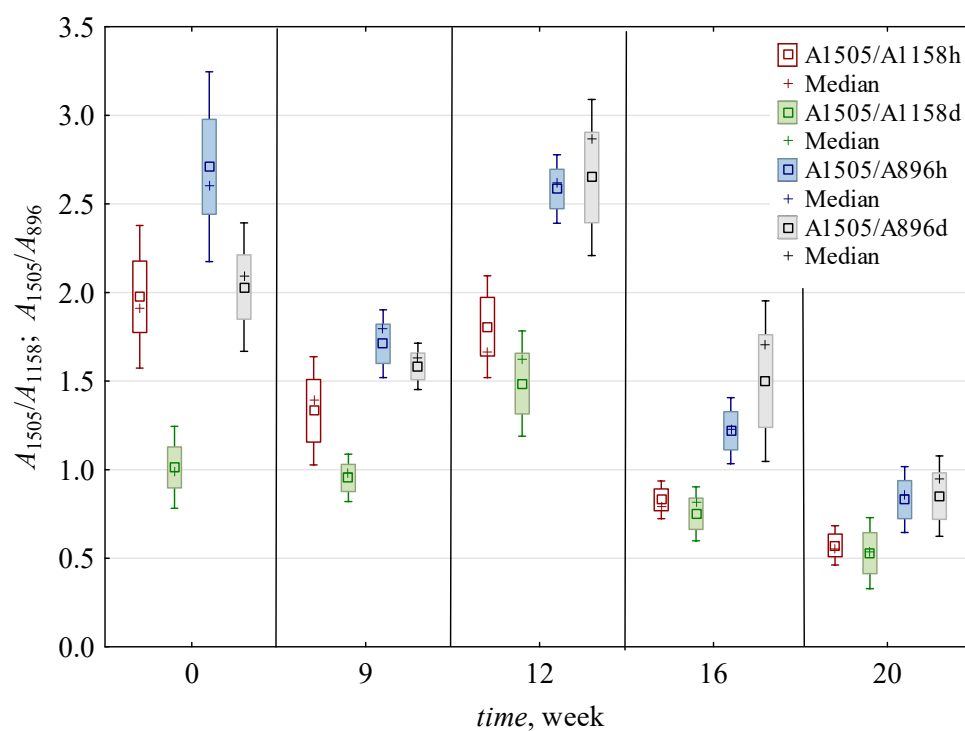
Figure 6. Values of ratios of absorbances for respective wavenumbers: A_{1505}/A_{1158} and A_{1505}/A_{896}; *h*—peak height, *d*—peak deconvolution, □—mean, frame—*SE*, and whisker—*SD*.
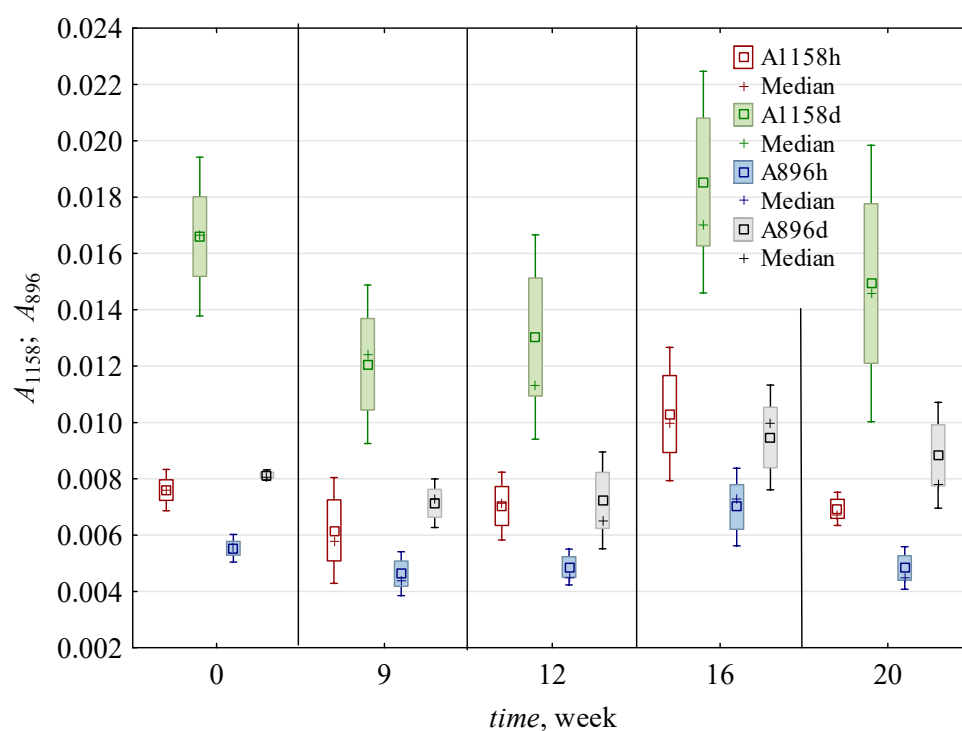

Figure 7. Value of absorbance A_{1158} for wavenumber characteristic for C–O–C vibrations in cellulose and hemicelluloses, and for A_{896} related to C–H deformation vibrations in cellulose; *h*–peak height, *d*—peak deconvolution, □—mean, frame—*SE*, and whisker—*SD*.

3.2.3. Delignification Based on Comparison with Cellulose

The A_{1505}/A_{896} ratio indicates the amount of lignin compared with cellulose. Values of this ratio, estimated from peak heights, changed similarly to A_{1505}/A_{1375}, presenting a decreasing trend, except from weeks 9 to 12 (Figure 4), and the correlation coefficient between these ratios was 0.586 (Table 2). Similarly, the A_{1505}/A_{896} ratio increase was caused by the aforementioned increase in the value of A_{1505} (Figure 3), which is demonstrated by the high correlation $r = 0.769$ (Table 2). A_{1505}/A_{896} ratio decreased from weeks 0 to 9, both for the numerator and denominator (Figs. 3 and 7). Later, in week 12, because of the decrease in the peak A_{1505} value (Figure 3), A_{1505}/A_{896} increased, and the A_{896} value (Figure 7) presented a minor change between weeks 9 and 12.

3.3. Changes in Indexes of Crystallinity

Values of *LOI* ratios calculated from peak heights and from deconvoluted spectra both decreased in week 9 (from 1.22 to 1.07, Table 2), increased to 1.31 in week 12, and decreased in week 16, plateauing until the end of experiment (Figure 8). Changes in *LOI* indicate increases in crystallinity to week 12 after its initial decrease. Next, from week 12, crystallinity decreased and later stabilised. The decrease in *LOI* in week 9 can be explained by lignin decomposition, as the value of A_{1420} is connected with the presence of methoxyl groups in lignin [32]. The influence of lignin on the decrease in *LOI* is supported by the simultaneous decrease in A_{1505} (Figure 3).
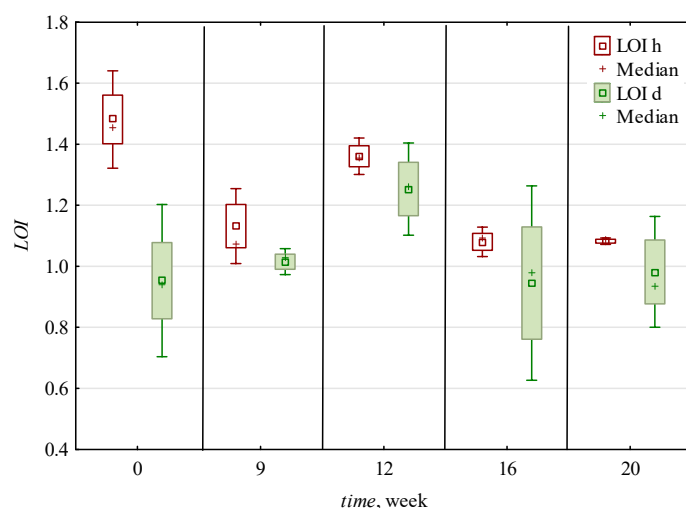

Figure 8. Values of *LOI; h*—peak height, *d*—peak deconvolution, □—mean, frame—*SE*, and whisker—*SD*.

Figure 9 shows changes in A_{1420}, a numerator of the *LOI* ratio. The value of A_{1420} decreased in week 9 from 0.008 to 0.006; it decreased to 0.008 in week 16; and a small decrease was observed in week 20. A decrease in A_{1420} in week 9 (Figure 2) reveals a reduction in crystallinity, and the degradation of hemicelluloses because A_{1420} originates, for example, from C–H vibrations in methoxyl groups in hemicelluloses [22]. Additionally, a decrease in this peak, which originates from –OCH$_3$ vibrations in lignin [32] or even whole fragments of lignin, is suggestive of lignin demethoxylation, as there is a simultaneous decrease in the A_{1505} value (Figure 3). The correlation between A_{1420} and A_{1505} is high, 0.618. Later changes were not consistent with changes in lignin and hemicellulose content, and additional research is required to explain this observation.
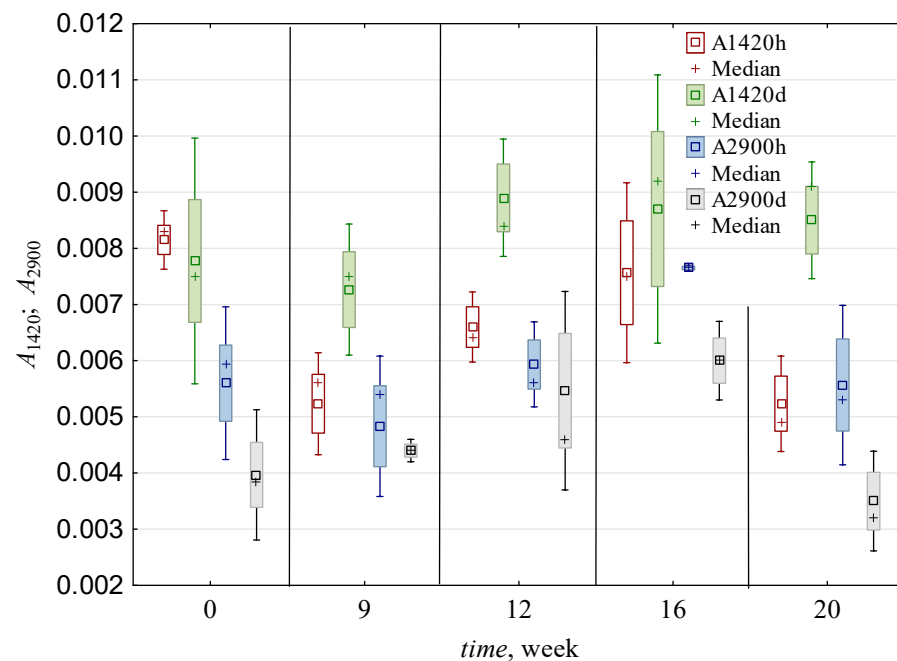
Figure 9. Value of A_{1420} absorbance for wavenumbers characteristic of CH_2 bending vibrations related to the crystalline fraction and for A_{2900} characteristic for CH_2 stretching vibrations related to the amorphous fraction; *h*—peak height, *d*—peak deconvolution, □—mean, frame—*SE*, and whisker—*SD*.

Indexes of Crystallinity

The *TCI* for broad baseline increased until week 12, from 1.45 to 1.65, and later decreased to 1.21, stabilizing to a near-plateau (Figure 10). *TCI* for a narrow baseline changed in a similar way (r = 0.954, almost full correlation, Table 3), but the average value was 19% lower than for the broad baseline. *TCI* calculated on the basis of deconvolution increased in week 9 and decreased irregularly until the end of experiment. The course of *TCI* suggests no changes in cellulose crystallinity in particleboard pretreated by *P. ostreatus*.
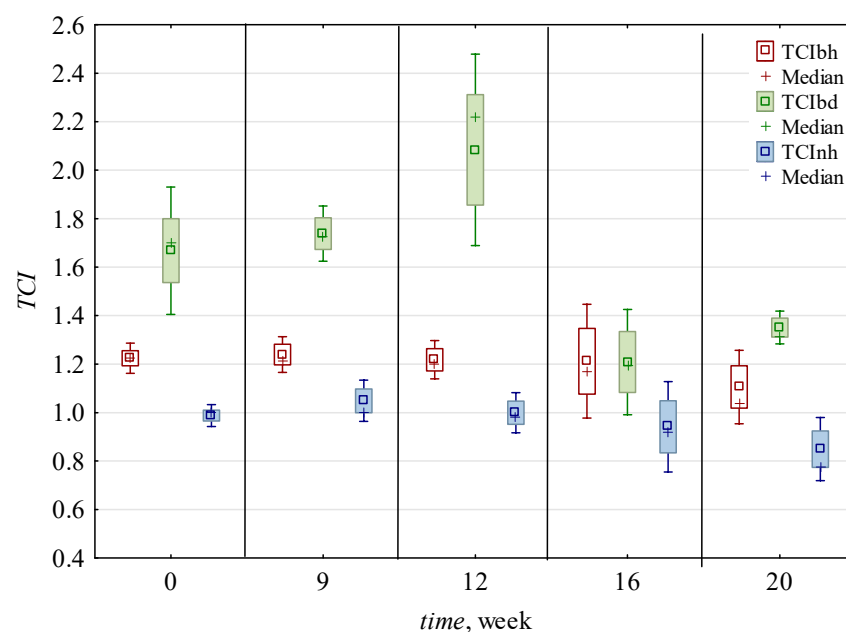

Figure 10. Values of *CI*: *b*—broad base, *n*—narrow base, *h*—peak height, *d*—peak deconvolution, □—mean, frame—*SE*, and whisker—*SD*.

The value of A$_{2900}$ (Figure 9), the denominator in TCI, was chosen to be the same for TCI calculated on the basis of A$_{1375}$ with broad and narrow baselines [30].

Generally, in the definition of *TCI*, A_{2900} was utilised as an internal standard because this peak is relatively unchanged in cellulose. For the internal standard, the influence of random scattering of radiation on particles in the sample and a different amount of analysed material in KBr pellets had to be minimised [30].

During the activity of *P. ostreatus*, changes in chemical bonds measured at A_{2900} cannot be excluded, so the utilisation of A_{2900} as an internal standard is doubtful. Moreover, particleboards with UF resin are not the same as those with pure cellulose, and changes in A_{2900} might depend on changes in other components of the particleboards.

As indexes of crystallinity, *LOI* and *TCI* were elaborated on the basis of research conducted on sole cellulose [30], so these indexes do not include the influences of other wood components, e.g., hemicelluloses and lignin. The influence of these components makes changes in crystallinity based on FTIR spectra difficult to interpret. It is recommended to extend the scope of this research by using other methods, which will allow more conclusive interpretation of the effects of particleboard pretreatment by *P. ostreatus*.

The values of $R = A_{1120}/A_{1078}$, another ratio connected with crystallinity, noticeably decreased in week 9 (from 0.75 to 0.61, Table 2), and similarly in week 12, and were thereafter almost unchanged until the end of the experiment (Figure 11).
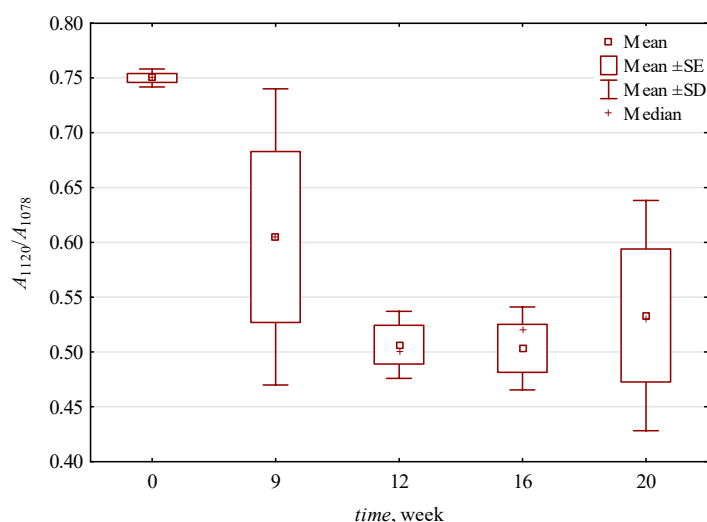

Figure 11. Values of crystallinity $R = A_{1120}/A_{1078}$ based on deconvolution.

3.4. Results of Feature Correlation Method

As high values of correlation coefficients between indexes suggested their redundance, some indexes were excluded: the amount of lignin compared with the amount of cellulose, A_{1505}/A_{896} (almost full correlation with A_{1505}/A_{1158}, $r = 0.912$); absorbance at A_{1735} (very high correlation with A_{1505}, $r = 0.803$); absorbance at A_{896} (almost complete correlation with A_{1158}, $r = 0.931$); the amount of lignin compared with the amount of holocellulose A_{1505}/A_{1375} (very high correlation with A_{1505}/A_{1735}, $r = 0.825$); absorbance at A_{2900} (high correlation with A_{1375b}, $r = 0.618$); and absorbance at A_{1158} (high correlation with A_{1420}, $r = 0.624$). Finally, seven indexes were used for pretreatment estimation: *LOI*; *TCIb* (for broad baseline); amount of lignin compared with hemicellulose, A_{1505}/A_{1735}; amount of lignin compared with holocellulose, A_{1505}/A_{1158}; and absorbances A_{1505}, A_{1420}, and A_{1375} for wavenumbers characteristic of lignin (1505 cm^{-1}), crystalline fraction (1420 cm^{-1}), and holocellulose (1375 cm^{-1}), respectively. This selection of criterial parameters, with the help of the feature correlation method [38], allows one to increase the perception of information processing and reveals important indexes for characterizing particleboard pretreatment by *P. ostreatus* at a sufficient level.

4. Conclusions

How to sufficiently utilise furniture industry wastes is an increasing problem, and a possible solution is to convert them into biofuels such as ethanol. However, this process requires pretreatment, which was conducted here.

The main factors of time and how to calculate indexes were found, in most cases, to be statistically important variables influencing the differentiation of indexes of particleboard pretreatment with *P. ostreatus*. The interaction time and the influence of indexes were determined to be statistically significant based on the absorbance of peaks at 1505, 1735, and 1375 cm^{-1} for the broad baseline along with the influences on the ratios A_{1505}/A_{1375} and A_{1505}/A_{1158} and *TCI* for the broad baseline.

Up to week 9, pretreatment seemed beneficial for biofuel production, e.g., decreases in values measured at 1735 and 1505 cm^{-1} values and A_{1505}/A_{1375}, A_{1505}/A_{1735}, A_{1505}/A_{1375}, A_{1505}/A_{1158}, and A_{1505}/A_{896} ratios were indicative of lignin and hemicellulose decomposition in addition to selective delignification by *P. ostreatus*. Similarly, positive changes were noticed in the case of crystallinity indexes (*LOI*, *TCI*, *R*). The breakdown of the direction of changes after week 16 might have been caused by the fungal defence being overcome, which occurred between weeks 16 and 20. Changes that occurred after week 9 of pretreatment should be analysed using different analytical methods, as FTIR does not allow one to formulate unequivocal conclusions.

Author Contributions: Conceptualization, J.G. and P.T.; methods, J.G., P.T. and B.A.; software, P.T. and A.L.; formal analysis, P.T., J.G. and A.L.; investigation, P.T., J.G., B.A. and A.O.; resources, P.T. and J.G; data curation, P.T. and J.G.; writing—original draft preparation, P.T.; writing—review and editing, J.G. and A.L.; visualization, P.T. and A.L.; project administration, J.G.; supervision, J.G. All authors have read and agreed to the published version of the manuscript.

Data Availability Statement: The data will be made available upon request.

Conflicts of Interest: The authors declare no conflict of interest.

References

1. CSO. *Statistical Yearbook*; CSO: Cork, Ireland, 2019.
2. Nemli, G.; Öztürk, I. Influences of some factors on the formaldehyde content of particleboard. *Build. Environ.* **2006**, *41*, 770–774. [CrossRef]
3. Szadkowska, D. Suitability of biomass from waste wood composites for liquid biofuel production Możliwość wykorzystania biomasy poużytkowych tworzyw drzewnych w technologii ciekłych biopaliw. *Przem. Chem.* **2015**, *1*, 74–76. [CrossRef]
4. Althuri, A.; Gujjala, L.K.S.; Banerjee, R. Partially consolidated bioprocessing of mixed lignocellulosic feedstocks for ethanol production. *Bioresour. Technol.* **2017**, *245*, 530–539. [CrossRef]
5. Agarwal, U.P.; Zhu, J.Y.; Ralph, S.A. Enzymatic hydrolysis of biomass: Effects of crystallinity, particle size, and lignin removal. In Proceedings of the 16th International Symposium on Wood, Fiber, and Pulping Chemistry—Proceedings, ISWFPC, Tianjin, China, 8–10 June 2011; Volume 2, pp. 908–912.
6. Yoshida, M.; Liu, Y.; Uchida, S.; Kawarada, K.; Ukagami, Y.; Ichinose, H.; Kaneko, S.; Fukuda, K. Effects of cellulose crystallinity, hemicellulose, and lignin on the enzymatic hydrolysis of Miscanthus sinensis to monosaccharides. *Biosci. Biotechnol. Biochem.* **2008**, *72*, 805–810. [CrossRef]
7. Ghasemzadeh, R.; Mosavian, M.T.H.; Karimi, A. Analysis of biological pretreatment of rapeseed straw with white rot fungi for enzymatic hydrolysis. *Maderas Cienc. Tecnol.* **2018**, *20*, 725–736. [CrossRef]
8. Phongpreecha, T.; Christy, K.F.; Singh, S.K.; Hao, P.; Hodge, D.B. Effect of catalyst and reaction conditions on aromatic monomer yields, product distribution, and sugar yields during lignin hydrogenolysis of silver birch wood. *Bioresour. Technol.* **2020**, *316*, 123907. [CrossRef] [PubMed]
9. Torr, K.M.; Love, K.T.; Simmons, B.A.; Hill, S.J. Structural features affecting the enzymatic digestibility of pine wood pretreated with ionic liquids. *Biotechnol. Bioeng.* **2016**, *113*, 540–549. [CrossRef]
10. Studer, M.H.; DeMartini, J.D.; Davis, M.F.; Sykes, R.W.; Davison, B.; Keller, M.; Tuskan, G.A.; Wyman, C.E. Lignin content in natural populus variants affects sugar release. *Proc. Natl. Acad. Sci. USA* **2011**, *108*, 6300–6305. [CrossRef]

11. Ohlsson, J.A.; Hallingbäck, H.R.; Jebrane, M.; Harman-Ware, A.E.; Shollenberger, T.; Decker, S.R.; Sandgren, M.; Rönnberg-Wästljung, A.C. Genetic variation of biomass recalcitrance in a natural *Salix viminalis* (L.) population. *Biotechnol. Biofuels* **2019**, *12*, 135. [CrossRef]

12. Healey, A.L.; Lupoi, J.S.; Lee, D.J.; Sykes, R.W.; Guenther, J.M.; Tran, K.; Decker, S.R.; Singh, S.; Simmons, B.A.; Henry, R.J. Effect of aging on lignin content, composition and enzymatic saccharification in Corymbia hybrids and parental taxa between years 9 and 12. *Biomass Bioenergy* **2016**, *93*, 50–59. [CrossRef]

13. Guo, F.; Shi, W.; Sun, W.; Li, X.; Wang, F.; Zhao, J.; Qu, Y. Differences in the adsorption of enzymes onto lignins from diverse types of lignocellulosic biomass and the underlying mechanism. *Biotechnol. Biofuels* **2014**, *7*, 38. [CrossRef] [PubMed]

14. Pimienta, J.A.P.; Papa, G.; Rodriguez, A.; Barcelos, C.A.; Liang, L.; Stavila, V.; Sanchez, A.; Gladden, J.M.; Simmons, B.A. Pilot-scale hydrothermal pretreatment and optimized saccharification enables bisabolene production from multiple feedstocks. *Green Chem.* **2019**, *21*, 3152–3164. [CrossRef]

15. Xu, J.K.; Sun, Y.C.; Sun, R.C. Synergistic effects of ionic liquid plus alkaline pretreatments on eucalyptus: Lignin structure and cellulose hydrolysis. *Process Biochem.* **2015**, *50*, 955–965. [CrossRef]

16. Govender, M.; Bush, T.; Spark, A.; Bose, S.K.; Francis, R.C. An accurate and non-labor intensive method for the determination of syringyl to guaiacyl ratio in lignin. *Bioresour. Technol.* **2009**, *100*, 5834–5839. [CrossRef]

17. Sequeiros, A.; Labidi, J. Characterization and determination of the S/G ratio via Py-GC/MS of agricultural and industrial residues. *Ind. Crops Prod.* **2017**, *97*, 469–476. [CrossRef]

18. Ding, D.; Zhou, X.; Ji, Z.; You, T.; Xu, F. How Does Hemicelluloses Removal Alter Plant Cell Wall Nanoscale Architecture and Correlate with Enzymatic Digestibility? *Bioenergy Res.* **2016**, *9*, 601–609. [CrossRef]

19. Ding, C.; Wang, X.; Li, M. Evaluation of six white-rot fungal pretreatments on corn stover for the production of cellulolytic and ligninolytic enzymes, reducing sugars, and ethanol. *Appl. Microbiol. Biotechnol.* **2019**, *103*, 5641–5652. [CrossRef] [PubMed]

20. Sahuand, S.; Pramanik, K. Evaluating fungal mixed culture for pretreatment of cotton gin waste to bioethanol by enzymatic hydrolysis and fermentation using co-culture. *Polish J. Environ. Stud.* **2017**, *26*, 1215–1223. [CrossRef]

21. Singh, T.; Vaidya, A.A.; Donaldson, L.A.; Singh, A.P. Improvement in the enzymatic hydrolysis of biofuel substrate by a combined thermochemical and fungal pretreatment. *Wood Sci. Technol.* **2016**, *50*, 1003–1014. [CrossRef]

22. Pandey, K.K.; Pitman, A.J. FTIR studies of the changes in wood chemistry following decay by brown-rot and white-rot fungi. *Int. Biodeterior. Biodegrad.* **2003**, *52*, 151–160. [CrossRef]

23. Li, M.; Marek, S.M.; Peng, J.; Liu, Z.; Wilkins, M.R. Effect of moisture content and inoculum size on cell wall composition and ethanol yield from switchgrass after solid-state *Pleurotus ostreatus* treatment. *Trans. ASABE* **2018**, *61*, 1997–2006. [CrossRef]

24. Schmidt, O. *Fundamentals of Mold Growth in Indoor Environments and Strategies for Healthy Living*; Springer: Berlin/Heidelberg, Germany, 2011; ISBN 9789086867226.

25. Vaverková, M.D.; Adamcová, D.; Radziemska, M.; Voběrková, S.; Mazur, Z.; Zloch, J. Assessment and Evaluation of Heavy Metals Removal from Landfill Leachate by *Pleurotus ostreatus*. *Waste Biomass Valorization* **2018**, *9*, 503–511. [CrossRef]

26. Pozdniakova, N.N.; Nikitina, V.E.; Turkovskaia, O.V. Bioremediation of oil-polluted soil with an association including the fungus *Pleurotus ostreatus* and soil microflora. *Prikl. Biokhim. Mikrobiol.* **2008**, *44*, 69–75. [CrossRef] [PubMed]

27. Singh, S.N. *Microbial Degradation of Synthetic Dyes in Wastewaters*; Environmental Science and Engineering; Sub Series Environmental Science; Springer: Berlin/Heidelberg, Germany, 2015; pp. iii–iv. [CrossRef]

28. El-Batal, A.I.; Elkenawy, N.M.; Yassin, A.S.; Amin, M.A. Laccase production by *Pleurotus ostreatus* and its application in synthesis of gold nanoparticles. *Biotechnol. Rep.* **2015**, *5*, 31–39. [CrossRef]

29. Chen, Y.; Fan, H.; Meng, F. *Pleurotus ostreatus* decreases cornstalk lignin content, potentially improving its suitability for animal feed. *J. Sci. Food Agric.* **2017**, *97*, 1592–1598. [CrossRef]

30. Nelson, M.L.; O'Connor, R.T. Relation of certain infrared bands to cellulose crystallinity and crystal lattice type. Part II. A new infrared ratio for estimation of crystallinity in celluloses I and II. *J. Appl. Polym. Sci.* **1964**, *8*, 1325–1341. [CrossRef]

31. Fabiyi, J.S.; McDonald, A.G.; Morrell, J.J.; Freitag, C. Effects of wood species on durability and chemical changes of fungal decayed wood plastic composites. *Compos. Part A Appl. Sci. Manuf.* **2011**, *42*, 501–510. [CrossRef]

32. Harrington, K.J.; Higgins, H.G.; Michell, A.J. Infrared Spectra of *Eucalyptus regnans* F. Muell. and *Pinus radiata* D. Don. *Holzforschung* **1964**, *18*, 108–113. [CrossRef]

33. Zhong, R.; Gu, J.; Gao, Z.; Tu, D.; Hu, C. Impacts of urea-formaldehyde resin residue on recycling and reconstitution of wood-based panels. *Int. J. Adhes. Adhes.* **2017**, *78*, 60–66. [CrossRef]

34. Yang, X.; Zeng, Y.; Ma, F.; Zhang, X.; Yu, H. Effect of biopretreatment on thermogravimetric and chemical characteristics of corn stover by different white-rot fungi. *Bioresour. Technol.* **2010**, *101*, 5475–5479. [CrossRef]

35. O'Connor, R.T.; Dupré, E.F.; Mitcham, D. Applications of Infrared Absorption Spectroscopy to Investigations of Cotton and Modified Cottons:Part I: Physical and Crystalline Modifications and Oxidation. *Text. Res. J.* **1958**, *28*, 382–392. [CrossRef]

36. Karimi, K.; Taherzadeh, M.J. A critical review of analytical methods in pretreatment of lignocelluloses: Composition, imaging, and crystallinity. *Bioresour. Technol.* **2016**, *200*, 1008–1018. [CrossRef] [PubMed]

37. Dong, X.Q.; Yang, J.S.; Zhu, N.; Wang, E.T.; Yuan, H.L. Sugarcane bagasse degradation and characterization of three white-rot fungi. *Bioresour. Technol.* **2013**, *131*, 443–451. [CrossRef] [PubMed]

38. Miller, G. The magical number seven, plus or minus two: Some limits on our capacity for processing information. *Psychol. Rev.* **1994**, *101*, 343–352. [CrossRef]

39. Hopkins, W.G. A New View of Statistics. *Sportscience* **2000**, 1–7. Available online: https://www.sportsci.org/resource/stats/newview.html (accessed on 29 October 2022).

40. Huang, X.; Korányi, T.I.; Boot, M.D.; Hensen, E.J.M. Ethanol as capping agent and formaldehyde scavenger for efficient depolymerization of lignin to aromatics. *Green Chem.* **2015**, *17*, 4941–4950. [CrossRef]

41. Pan, H. Wood Liquefaction in the Presence of Phenol With a Weak Acid Catalyst and Its Potential for Novolac Type Wood Adhesives. Ph.D. Thesis, Louisiana State University, Baton Rouge, LA, USA, 2007; pp. 1–109.